Indian Geotech J (August 2024) 54(4):1174–1186
https://doi.org/10.1007/s40098-023-00782-9

ORIGINAL PAPER

A Numerical Study on the Effect of Different Tunnel Shapes in Squeezing Rocks

H. Manasa[1,2] · **V. B. Maji**[2]

Received: 12 August 2022 / Accepted: 22 September 2023 / Published online: 8 November 2023

Abstract Squeezing failure is commonly observed when excavating tunnels in weak rocks in high in situ stress conditions. When the existing rock is removed from the rock mass, the in situ stresses redistribute itself, resulting in possible overstressing in the proximity of excavation with excessive deformation, which ultimately may lead to failure. Avoiding squeezing type failure is always a serious concern in tunnelling and is a field of active research for decades. Researchers have come out with several solutions for the quantification of squeezing and the corresponding failure in squeezing type rocks. Despite many studies, squeezing failure is unavoidable because most of the solutions might be lacking in comprehensive input parameters in reference to real-field conditions that influence excessive tunnel deformation. In the present study, key influencing parameters such as tunnel shape, in situ stress and rock mass characteristic are considered while doing numerical studies. Three tunnel shapes are analysed using the numerical tool *FLAC* under varying the above-mentioned parameters. The behaviour of rock mass is observed subjected to varying parameters, and the conclusion is drawn based on the obtained results.

Keywords Tunnel · Squeezing rock · Stresses · *FLAC* · GSI · Overburden · Plastic zone radius · Tunnel strain

✉ H. Manasa
manasah.7@bub.ernet.in

[1] Department of Civil Engineering, UVCE, Bangalore University, Bengaluru, Karnataka, India

[2] Department of Civil Engineering, IIT-Madras, Chennai, TamilNadu, India

Introduction

Squeezing failure during tunnelling in weak rocks is always a serious problem in Himalayan region of India because of its frequently changing geology with rock formations of different ages. This squeezing phenomenon was defined by Weismann in 1912 as the redistribution of stresses and formation of a plastic zone around a deep tunnel [1]. Overstressing in the proximity of excavation may be one of the reasons leading to squeezing rock failure [2]. As per much of the literature, when the deformation of an unsupported opening exceeds 1% of the size of the opening, the ground is characterized as the squeezing ground which results in constructional problems [2–4]. Muirwood proposed an analytical approach using the 'competency factor' to estimate the tunnel stability, and the competency factor is defined as the ratio of uniaxial strength to overburden stress [5].

$$\text{Competency factor} = \frac{\text{uniaxial strength}}{\text{OB stress}} \tag{1}$$

Analyses using an axisymmetric orthotropic elastic model and an elastoplastic model on tunnels in squeezing rock mass provided a qualitative explanation of the mode of deformation and buckling failure. But getting quantitative results is very complex because of the lack of data on geomechanical characteristics of rock mass and the natural state of stress [6]. Rock mass properties and in situ stresses play an important role in triggering the failure in massive rock mass [7]. The risk of tunnel failure can be minimized in certain cases by the use of numerical analyses with appropriate rock mass parameters [8]. Detailed numerical analyses were performed by a few researchers using the finite element method [9, 10] and the boundary element method [11]. Tunnel failure due to overstressing of the surrounding rock mass depends upon the

characteristics of the rock mass, the magnitude and direction of the in situ stresses, the shape of the tunnel and intensity and the orientation of the discontinuities [7]. The load imposed on support installed behind the tunnel face can be estimated by convergence confinement method (CCM) which is composed of three basic components, namely (i) the longitudinal deformation profile (LDP), (ii) the ground reaction curve (GRC) and (iii) the support characteristic curve (SCC) [12]. CCM is a continuous approach that does not take into account rock wedges and one of the difficulties in applying this approach is defining how to adequately characterize strain-softening rock masses [13]. The empirical methods proposed by several researchers [3, 14–18] to quantify squeezing potential indicate that the approaches are general estimates of squeezing [19]. The nature of in situ stresses and their redistribution upon excavation play a crucial role in inducing tunnel instability problems in the rocks prone to squeezing type failure. Hence, this study presents the effect of isotropic in situ stresses on three different tunnel shapes upon varying geological strength index (GSI) of rock mass and varying overburden (OB) depth.

In the present paper, a hypothetical model is built of three different tunnel shapes using numerical tool *FLAC* and each tunnel is analysed under varying overburden and GSI under isotropic stress state. Tunnel strain and radius of plastic zone are determined for the above mentioned conditions.

Numerical Model

The analyses are performed using a numerical tool *FLAC* (Fast Lagrangian Analysis of Continua), a two-dimensional explicit finite difference-based numerical tool. *FLAC* contains a powerful built-in programming language *FISH*, through which tunnel closure and deformational behaviour of the tunnel can be analysed. *FLAC* is a continuum model, which uses the mixed discretization scheme for accurate modelling of physical collapse loads and plastic flows, whereas the explicit scheme can follow arbitrary nonlinearity in stress/strain laws [20]. The rock mass is considered as a continuous medium in the present squeezing analysis considering the generalized Hoek–Brown (GHB) model (Eq. 2). GHB model is an alternative to the Hoek–Brown (HB) [20, 21] model which allows the user to specify dilation options and include tensile strength limit. GHB parameters s, a and m_b can be found using intact rock characteristics and rock mass classification using geological strength index (GSI) (Eqs. 3, 4 and 5) [20]. The present study does not include the dilation behaviour of the rock mass.

$$\sigma_1 = \sigma_3 + \sigma_{ci}\left(m_b\frac{\sigma_3}{\sigma_{ci}} + s\right)^a \tag{2}$$

where σ_1 = major principle effective stress at failure, σ_3 = minor principle effective stress at failure, σ_{ci} = UCS of intact rock, m_b, s and a = Hoek and Brown material parameters which are functions of "D" (disturbance factor) and GSI (geological strength index).

$$m_b = m_i \exp\left(\frac{\mathrm{GSI} - 100}{28 - 14D}\right) \tag{3}$$

$$s = \exp\left(\frac{\mathrm{GSI} - 100}{9 - 3D}\right) \tag{4}$$

$$a = \frac{1}{2} + \frac{1}{6}\left(e^{-\mathrm{GSI}/15} - e^{-20/3}\right) \tag{5}$$

Here, m_i represent intact rock parameter which is selected based upon the range of values available for intact rocks.

For verification purposes, a case study has been considered namely the nuclear power generating station located on the shore of Lake Ontario near Toronto constructed in 1982. The tunnel named, 'Darlington' is excavated in limestone rock mass using drill and blast method with inverted-D shape opening of 9 m span and 92 m length with varying overburden of 21 m to 36 m [22]. The study considers *GHB* constitutive model, and corresponding inputs parameters are presented in Table 1 which are generated from RocLab software with the available parameters [22]. The state of in situ stress is remarkably anisotropic with a stress ratio of 10. The plane strain method is adopted where the displacements along the domain boundary are restrained in a direction perpendicular to the boundary. Anisotropic initial stresses are initialized in the model. The geometry of the model is shown in Fig. 1a. Obtained results show high inward horizontal displacement at the tunnel walls and less displacement at the crown and invert (Fig. 1b). Obtained displacements along crown and springline are compared with the displacements measured at the field (Fig. 2) and are found consistent with those observed values [5].

Numerical Analyses

Numerical analyses are performed by considering a simple tunnel model to observe the influence of factors such as tunnel shape, material property, overburden depth and isotropic in situ stress for unsupported tunnel. Figure 3 shows

Table 1 Rock mass parameters for Darlington tunnel [22, 23]

Compressive strength of rock mass, σ_{cm} (MPa)	80
Poisson's ratio	0.33
Young's modulus, E (GPa)	30
Tensile strength, σ_t (kPa)	4
GSI (geological strength index)	80

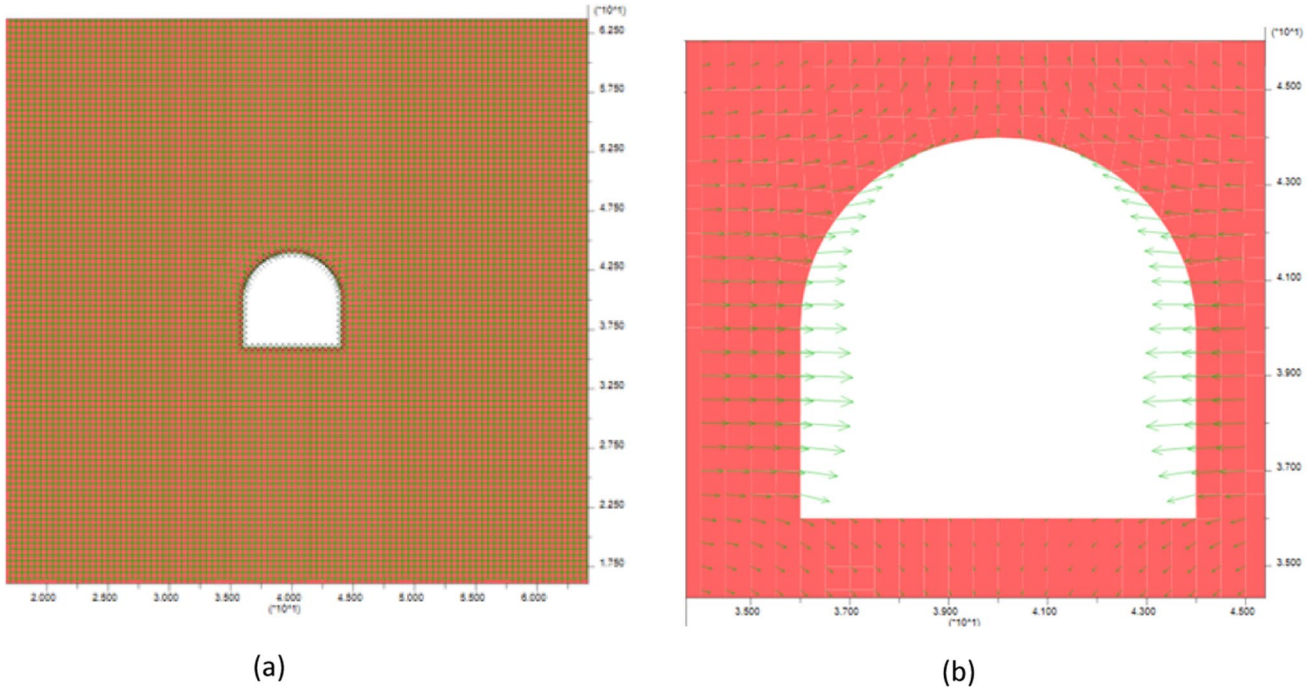

Fig. 1 **a** Geometry and **b** Obtained displacement pattern using FLAC

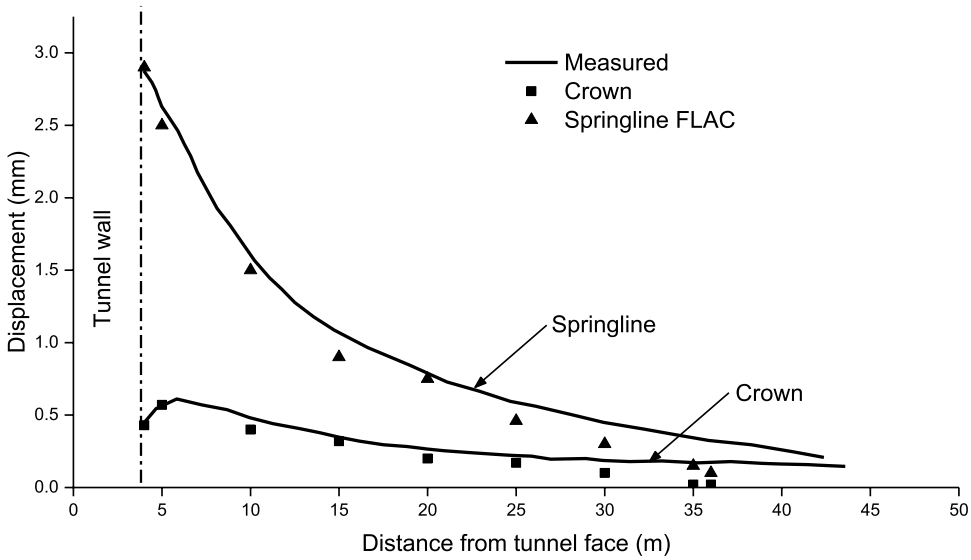

Fig. 2 Measured and obtained displacements for Darlington tunnel

commonly adopted terminology in tunnelling and the same is followed in the entire discussion of this paper. Three tunnel shapes are considered here namely, circular, inverted-D and horse-shoe shape (Fig. 4). The analyses are performed to observe the tunnel closure and extent of plastic zone radius for all the three tunnel shapes under varying overburden depths, isotropic stress condition and material properties. Focus of the study is to understand the behaviour of tunnels excavated in squeezing rock mass. Since squeezing failure is observed in a weak rock mass [3, 24–28] such as shale, limestone, gneiss with low strength, parameters for the present study are taken after a review of several tunnel case histories which underwent squeezing failure [2, 3, 7, 25–29]. Since the present simulation adopts the generalized Hoek–Brown constitutive model (Eq. 1.2), where all the parameters of this equation are influenced by GSI, the main focus in varying material properties is performed by considering different GSI values. The remaining relevant parameters of the *GHB*

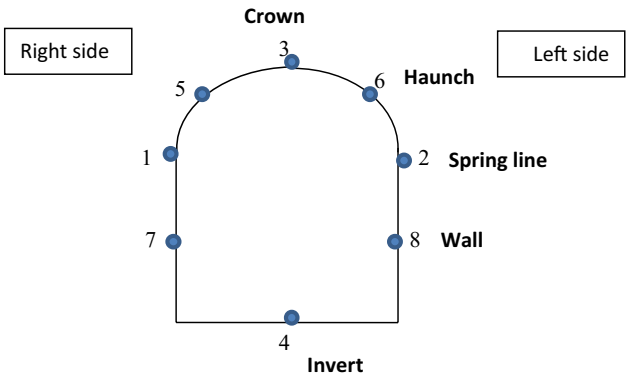

Fig. 3 The terminology used in tunnelling

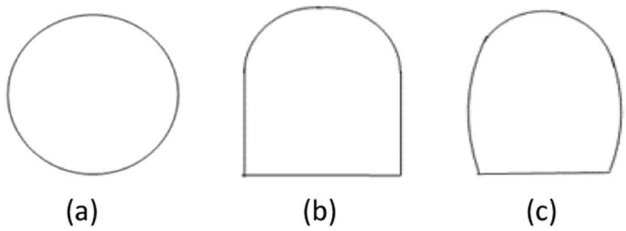

Fig. 4 Three tunnel shapes of hypothetical model. **a** Circular, **b** Inverted-D and **c** Horse-shoe

model are obtained by RocLab. Since squeezing failure in tunnels is associated with weak rocks (GSI < 30) to medium-strength rocks (GSI > 30) and also it was observed that the GSI of rock mass where squeezing failure was encountered ranges from 5 to 43 [3, 7, 26–29], values of GSI in this study are varied from 10 to 40 in an interval of 10, where an average of three GSI is considered as shown in Table 2. Tunnel overburden depths of 100 m, 300 m, 500 m, 600 m, 800 m and 1000 m are considered which are the average values of 50 m on either side for each overburden depth.

FLAC is an explicit code and hence solution to the problem requires several computational steps to reach the static solution stage (a state at which the model will be either in force equilibrium or a state of steady-flow of material). Since the objective is to analyse and comprehend unsupported tunnel behaviour subjected to varying overburden depth and material properties, calculation steps are kept constant for all the different cases considered. Two calculation steps are given for each case in such a way that the behaviour of rock mass within its yield limit and the behaviour at or after crossing the yield limit are observed. In this study, the tunnel is first checked under 150 calculation steps to show its behaviour before reaching yield limit (Before failure); later, it is verified under 500 calculation steps to observe the behaviour when it reaches or crosses the yield limit (when failure occurs/tunnel collapse).

The change in tunnel load that takes place due to tunnel excavation is simulated by the method of relaxation of forces where tractions are first applied to the tunnel boundary to provide an equilibrium condition at zero relaxation, and then tractions are gradually reduced. Since in reality, some relaxation of tunnel load takes place upon excavation, in the present research work 100% relaxation is considered. The same procedure is followed for all the tunnel shapes under varying conditions. For building the mesh, a domain size of 20D (twenty times the tunnel width) is considered because the extent of the failure zone is larger in squeezing conditions. Since the tunnel width is kept constant at 5 m, the geometry of the model is built of size 100 m × 100 m with 16,900 grids. The behaviour of rock mass around the vicinity of the tunnel is of prime importance and hence to obtain accurate results in this region, denser grids are assigned, whereas the grid size increases as it moves a certain distance away from the vicinity of the tunnel excavation. A quarter portion of the geometry of the circular tunnel with increasing grid size is shown in Fig. 5. The geometry of the numerical model (zoomed in) for three tunnel shapes is shown in Fig. 6.

Results and Discussion

Obtained results for all the three tunnel shapes under varying overburden depths and different GSI values are shown in Figs. 7, 8 and 9. The analyses are performed in two stages, firstly when the tunnel is within failure limits and then secondly when the tunnel reaches failure limit as explained in "Numerical Analyses" section. The behaviour in both cases for all the three tunnel shapes are observed to be different.

Table 2 Average GSI and overburden depths considered for the study

GSI				Overburden (OB) (m)					
GSI	Mean	GSI	Mean	OB	Mean	OB	Mean	OB	Mean
5	10	25	30	50	100	450	500	750	800
10		30		100		500		800	
15		35		150		550		850	
15	20	35	40	250	300	550	600	950	1000
20		40		300		600		1000	
25		45		350		650		1050	

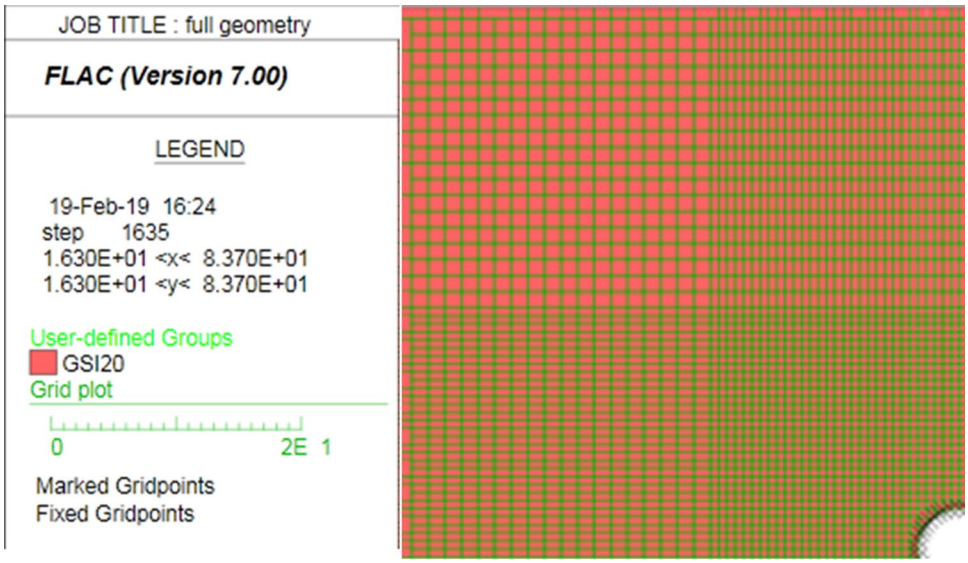

Fig. 5 Geometry of the model with increasing grid size from circular tunnel boundary

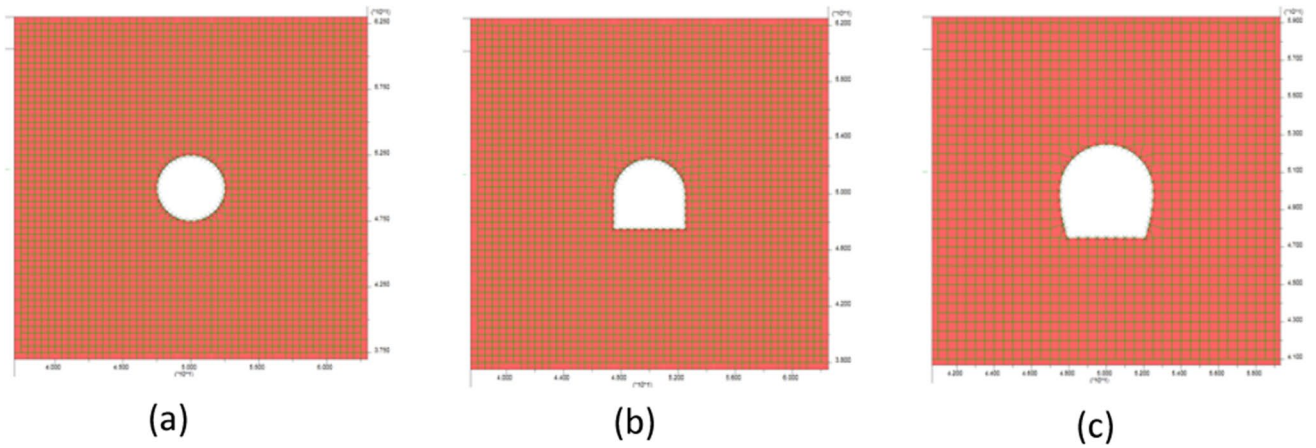

Fig. 6 Geometry of numerical model for three tunnel shapes. **a** Circular, **b** Inverted-D and **c** Horse-shoe

Tunnel strain is calculated by dividing the obtained tunnel closure by tunnel width/diameter. The concept of an increase in tunnel strain with respect to a decrease in GSI value at different overburden depths is valid only when the tunnel is within the failure limit. Because of isotropic stress conditions, tunnel convergence of circular tunnels in the horizontal and vertical directions is equal. It was observed that in a circular tunnel, the rock mass with GSI 10 can sustain an overburden height of 200 m. If the overburden depth is further increased, the tunnel is on the verge of failure (Fig. 7b). The rock mass with GSI 20 fails at or above 500 m overburden depth, whereas tunnel failure at or above overburden depth of 800 m was observed for rock mass of GSI 30, whereas the tunnel driven in rock mass of GSI 40 is stable even at strain of 14% (Fig. 7b) with overburden 1000 m. These obtained results indicate that the circular tunnel is stable even after reaching strain above 12% when the GSI of rock mass is 40 and above, whereas the rock mass with GSI 30 and below undergoes failure as the overburden depth increases.

As expected, the obtained results show that as the GSI value increases, tunnel strain decreases and the tunnels with higher GSI values can take higher strain before failure. Tunnel strain increases with increasing overburden depths for all GSI when the tunnel is within the yield limit.

Horizontal tunnel strains are measured at the sidewall and spring, whereas vertical tunnel strain is measured at the centre of the crown and invert for inverted-D shape and horse-shoe shape tunnel. The obtained strains indicate that as the overburden depth increases, strain at tunnel wall increases when compared to horizontal strain at spring and vertical strain (Fig. 8b). Obtained horizontal tunnel strain at spring and vertical tunnel strain are almost equal (Fig. 8b). Similar behaviour was observed

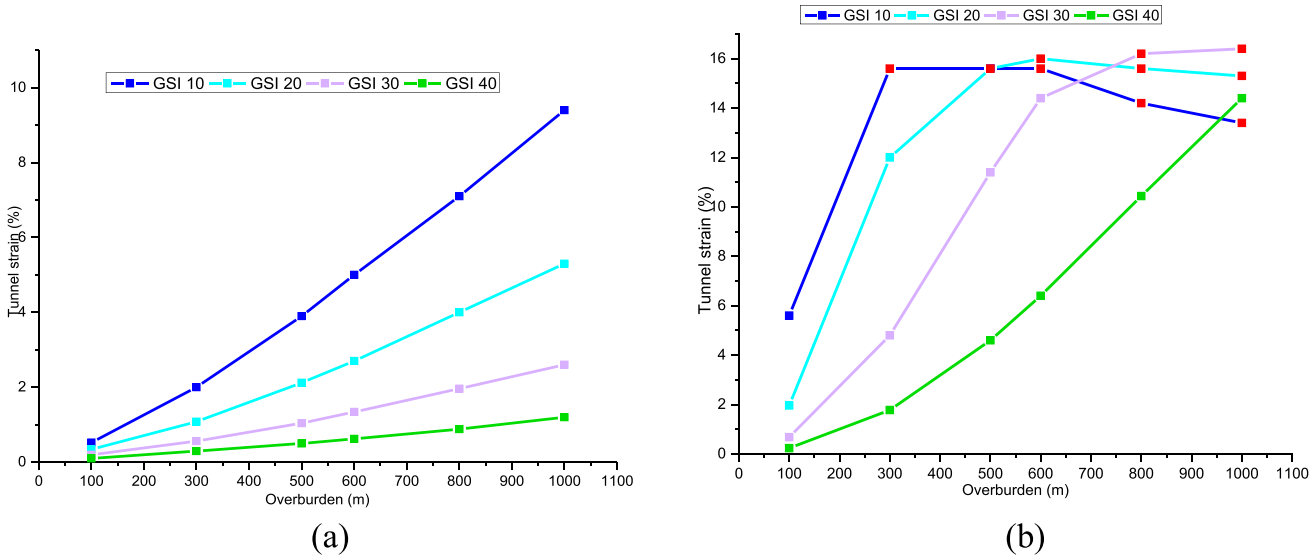

Fig. 7 Tunnel strains for the circular tunnel. **a** Within failure limit and **b** Until failure

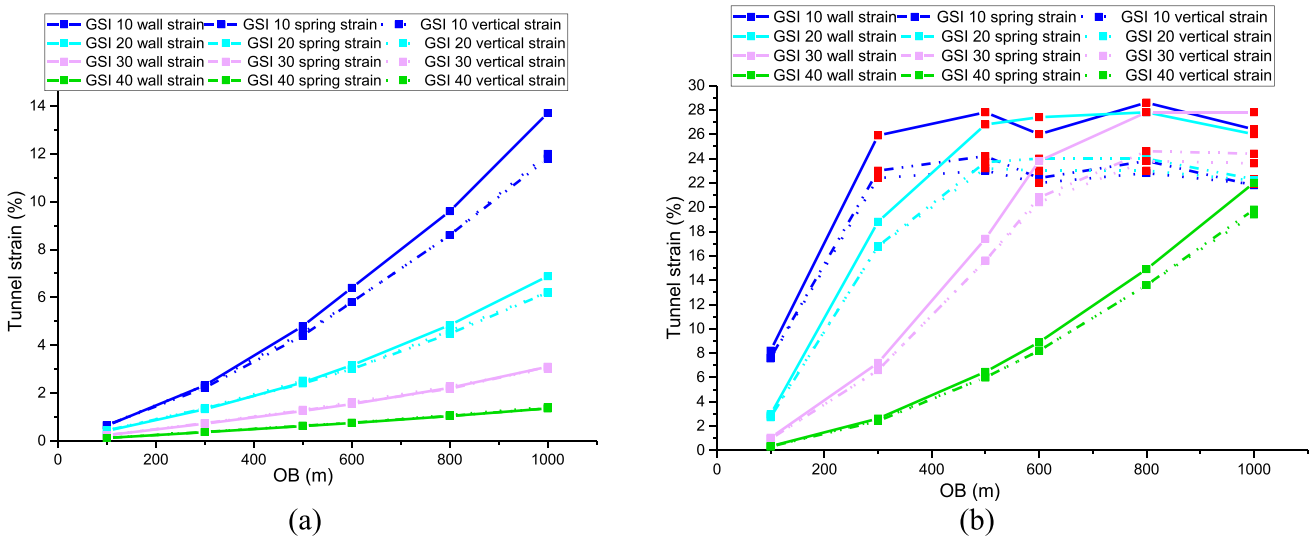

Fig. 8 Tunnel strains for inverted-D tunnel. **a** Within failure limit and **b** Until failure

for the Horse-shoe shape tunnel (Fig. 9b). Observations with inverted-D tunnel reveal that tunnel with GSI 10 fails under overburden depth of 300 m and above which indicate that these tunnels cannot take higher tunnel loads; however, upon an increase in overburden, the strain will not decrease (Fig. 8b), whereas in the horse-shoe tunnel, the strains will decrease when overburden depth is increased beyond 300 m (Fig. 9b) exhibiting behaviour similar to circular tunnel (Fig. 9b). Tunnel with GSI 20 fails at overburden depth of 500 m and above, whereas tunnel with GSI 30 fails at overburden depth of 800 m and higher. However, no failure is observed for tunnel driven with rock mass of GSI 40 (Fig. 8b) showing similar behaviour as that of the circular tunnel (Fig. 8b).

Similar behaviour is observed for the horse-shoe tunnels (Fig. 9b). It was observed for both inverted-D tunnel and horse-shoe tunnel that tunnel strain increase as overburden depth increases (Figs. 8a, 9a) when the tunnel is within yield zone but contrary to GSI value, i.e. as GSI value decreases, tunnel strain increases. Here also it was observed that the tunnel driven in rock mass of GSI 40 is stable at all overburden depths, whereas failure was observed at an increasing depth of overburden for GSI < 40 (Figs. 8b, 9b). Hence, it was concluded from the observations that the tunnel strain

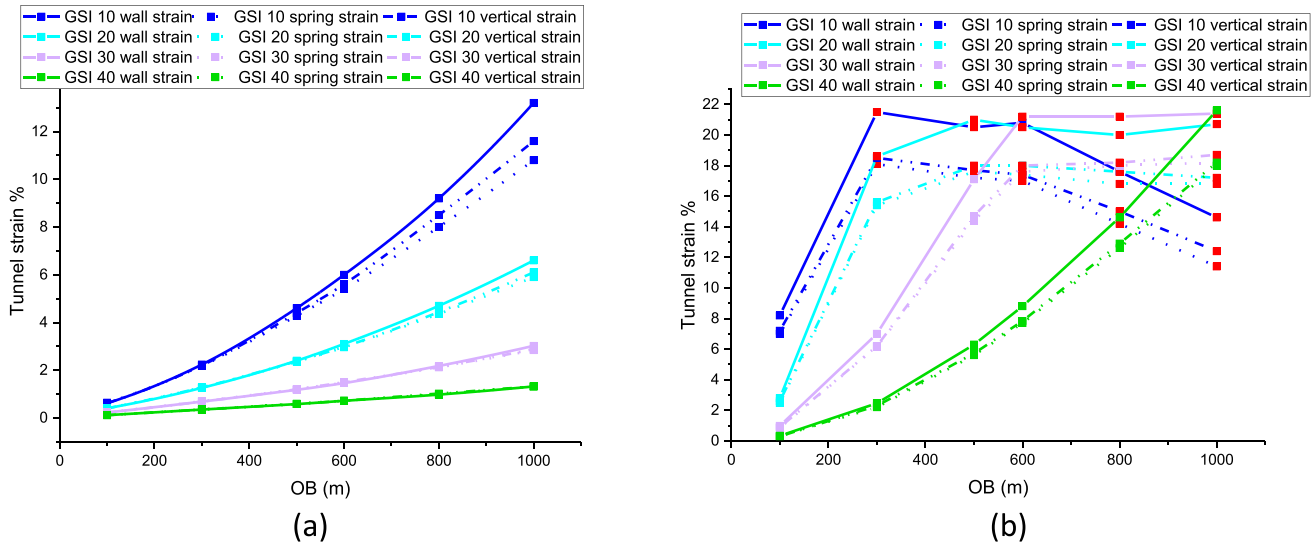

Fig. 9 Tunnel strains for horse-shoe tunnel. **a** Within failure limit and **b** Until failure

at failure not only depends on overburden depth but also on the material strength.

Tunnel inward displacement, the radius of plastic zone and stress conditions for all three tunnel shapes for varying overburden depths and GSI values are observed. Figure 10 shows one such observation for three tunnels at an overburden depth of 100 m with GSI 20. The radius of plastic zone is measured from the centre of the tunnel along spring and crown for circular tunnel, whereas for inverted-D and horse-shoe tunnel it is measured from tunnel centre along spring, wall, crown and invert. Inward displacement observed for all three tunnels shows that the entire tunnel cross section is displacing inward exhibiting squeezing type failure (Fig. 10a–c). The radius of the plastic zone for the circular tunnel is circular (Fig. 10d) with a radius equal to 3.8 m which exhibit the plastic zone around the tunnel opening. The rock mass beyond 3.8 m exhibits elastic behaviour. Because of the circular shape plastic zone, its radius is same both in horizontal and vertical directions of the tunnel. Influence of overburden depth and GSI of rock mass on the radius of the plastic zone for the circular tunnel is shown in Fig. 11. It is observed that for GSI < 30, tunnel fails at higher overburden depth of 300–500 m and above. Hence, plastic zone is disrupted because the tunnel has already crossed failure limit hence shown decline in the radius of the plastic zone (Fig. 11). For GSI ≥ 30, the radius of the plastic zone increases if no tunnel failure is observed, whereas for the tunnel that crosses the failure limit, the plastic zone is not disrupted and remains constant (Fig. 11). Hence, it can be stated that special consideration is required for tunnel excavated in squeezing rock of GSI < 30 of overburden depth 300 m and higher.

The plasticity zone for inverted-D tunnel and horse-shoe shape tunnel is in mushroom shape with symmetry along the vertical axis (Fig. 10e, f). Also, it is observed that the radius of the plastic zone is not equal in the horizontal and vertical direction which reads the value of 4.3 m at wall and spring, whereas invert exhibits 4.8 m radius which is more than the radius of 3.8 m at the crown for inverted-D tunnel (Figs. 10e, 11) and hence its radius is measured at two points along horizontal direction, namely at the wall, spring and at two points along vertical direction, namely at invert and crown (Fig. 12). The obtained radius of the plastic zone for inverted-D tunnel along horizontal (wall and spring) and vertical (invert and crown) direction is shown in Fig. 12a, b, respectively. It is observed that the zone of plasticity is higher at invert and wall when compared at spring and crown (Fig. 12a, b). The remarks made for the circular tunnel for GSI < 30 and GSI ≥ 30 imply for inverted-D tunnel as well. In a horse-shoe shape tunnel, the radius of the plastic zone at invert is higher when compared at the other three places (crown, wall and spring) along with tunnel opening (Fig. 13a, b). The behaviour of the plastic zone radius for GSI < 30 and GSI ≥ 30 is same as explained for the circular tunnel. Hence, engineers should be careful when designing tunnel running in squeezing rock of GSI < 30 with high overburden. As the tunnel excavation proceeds, the in situ state of stress redistributes resulting with deformation of surrounding rock, and the plastic zone which affects the stability of surrounding rock will gradually develop. In the present paper, isotropic stresses are considered; however practically, stresses do not remain isotropic all time. Hence, knowledge on behaviour of rock mass subjected to anisotropic stresses upon excavation is important.

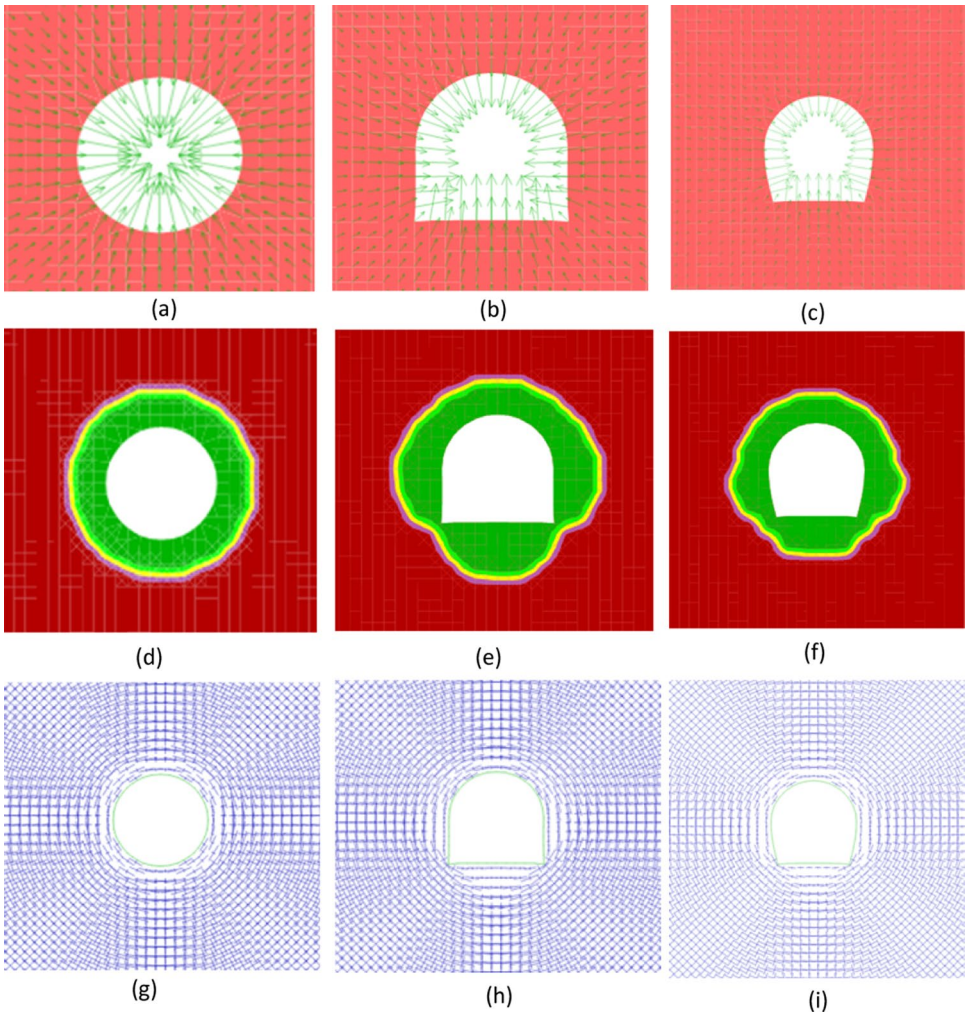

Fig. 10 **a**, **d**, **g** Displacement, radius of the plastic zone and principal stress distribution for circular tunnel, respectively; **b**, **e**, **h** Displacement, radius of the plastic zone and principal stress distribution for inverted D tunnel, respectively; **c**, **f**, **i** Displacement, radius of the plastic zone and principal stress distribution for horse-shoe tunnel, respectively

Tangential and Radial Stress Distribution

The state of stress in the rock mass is in equilibrium state before excavation, whereas stress redistribution takes place in the surrounding rock mass after excavation. Strength of the surrounding rock decreases, radial stress reduces and reach zero value in certain cases at the vicinity of excavation and then gradually increases along with the radial distance of tunnel and approaches to in situ stress value at the elastic region of rock mass after crossing plastic zone. The tangential stress also decreases at the tunnel boundary; however, because of tangential stress concentration, stress increases at a certain distance from the tunnel boundary within the zone of plasticity, then gradually decreases and approaches the in situ stress value far away from the plastic zone (in the elastic region). The influence range of distributed stress on the surrounding rock is limited. The stress distribution in the surrounding rock tunnel and the size of the plastic zone is very important in designing adequate support for the tunnel in squeezing rock. Tangential stress and radial stress distribution are obtained at spring and crown for circular tunnel, whereas for inverted-D tunnel and horse-shoe shape tunnel, it is obtained at spring, wall and crown.

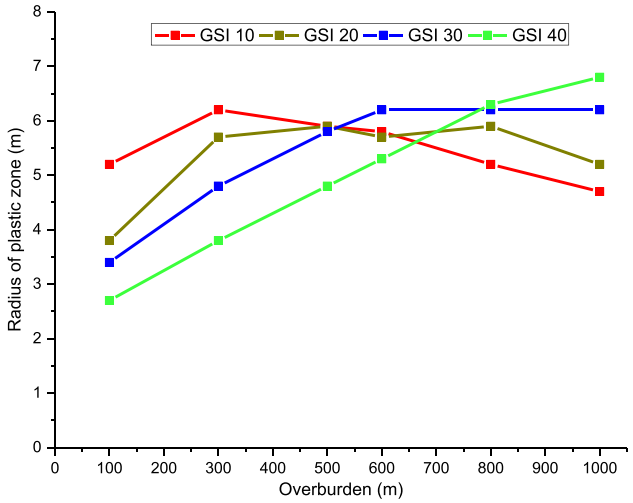

Fig. 11 The radius of plastic zone around circular tunnel

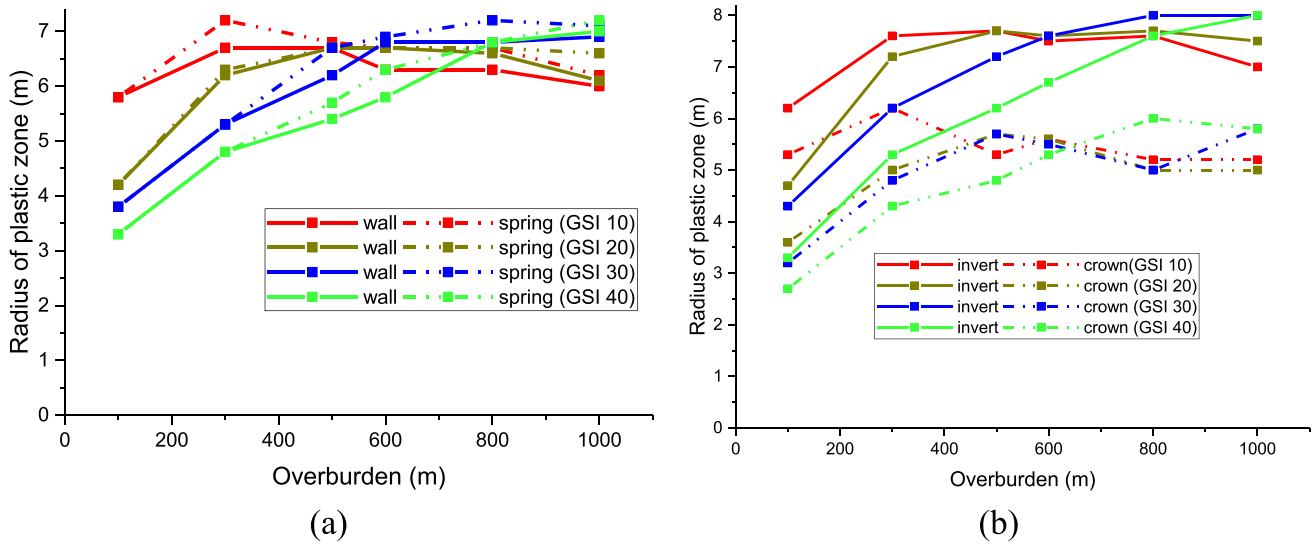

Fig. 12 The radius of plastic zone around inverted-D tunnel at **a** Wall and spring, **b** Invert and crown

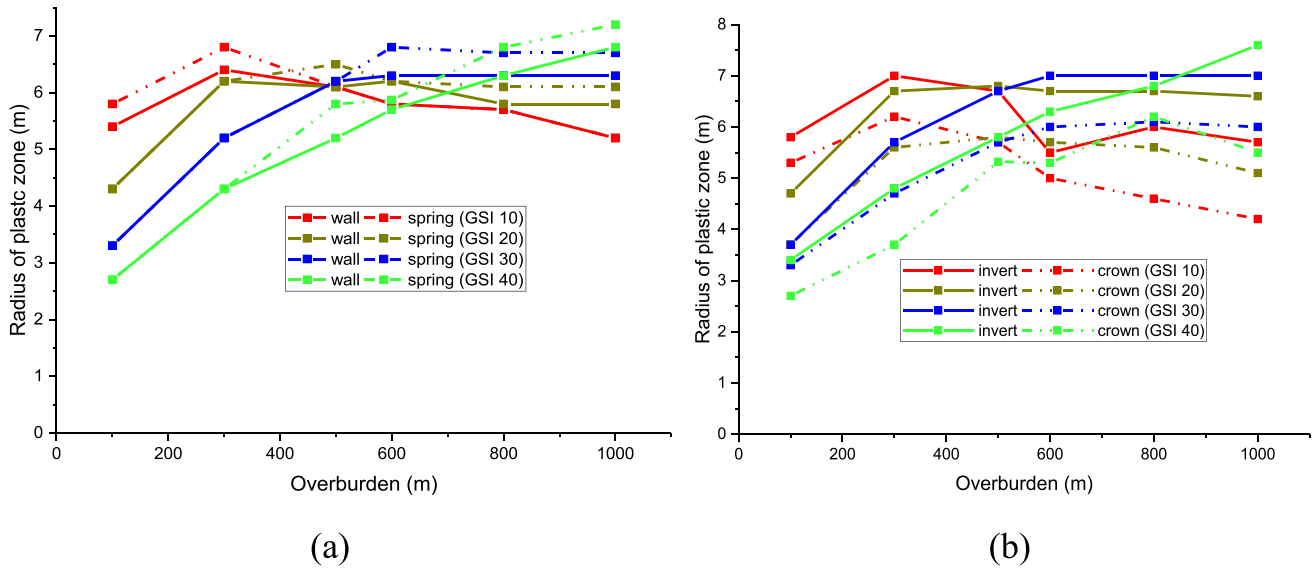

Fig. 13 The plot of the radius of the plastic zone around the horse-shoe tunnel at **a** Wall and spring, **b** Invert and crown

Distribution of radial and tangential stress along the radial distance of 30 m from the tunnel boundary around the vicinity of the circular tunnel for increasing overburden depth and GSI of 10 is shown in Fig. 14a, b. It is observed that the range of radial stress at the tunnel boundary is very less which gradually increases and approaches in situ state of stress at a radial distance of 12.5 m (5 times tunnel radius) from tunnel boundary for overburden of 100 m, whereas the radial distance at which radial stresses reach in situ state of stress increases to around 22 m for overburden depth 300 m and higher (Fig. 14a, b). Tangential stress at tunnel boundary is lesser than in situ stress and then increases more than in situ stress at a radial distance of 2.5–3 m for all the overburden depths and then gradually decreases and approaches to in situ stress at the same radial distance as explained for radial stress distribution (Fig. 14a, b). Similar behaviour is observed for inverted-D tunnel and horse-shoe shape tunnel. Radial and tangential stress distribution at crown occurs at a short radial distance when compared to wall and spring. The tangential stress for inverted-D tunnel at overburden depth of 100 m is a little higher than circular and horse-shoe shape tunnel. The behaviour of tangential and radial stress distribution along the radial distance is same as that explained for circular tunnels. It is observed that the influence range of distributed stresses decreases for higher GSI values showing tangential stress concentration is a little higher and it is moving towards the tunnel boundary along with radial distance as the GSI value increases.

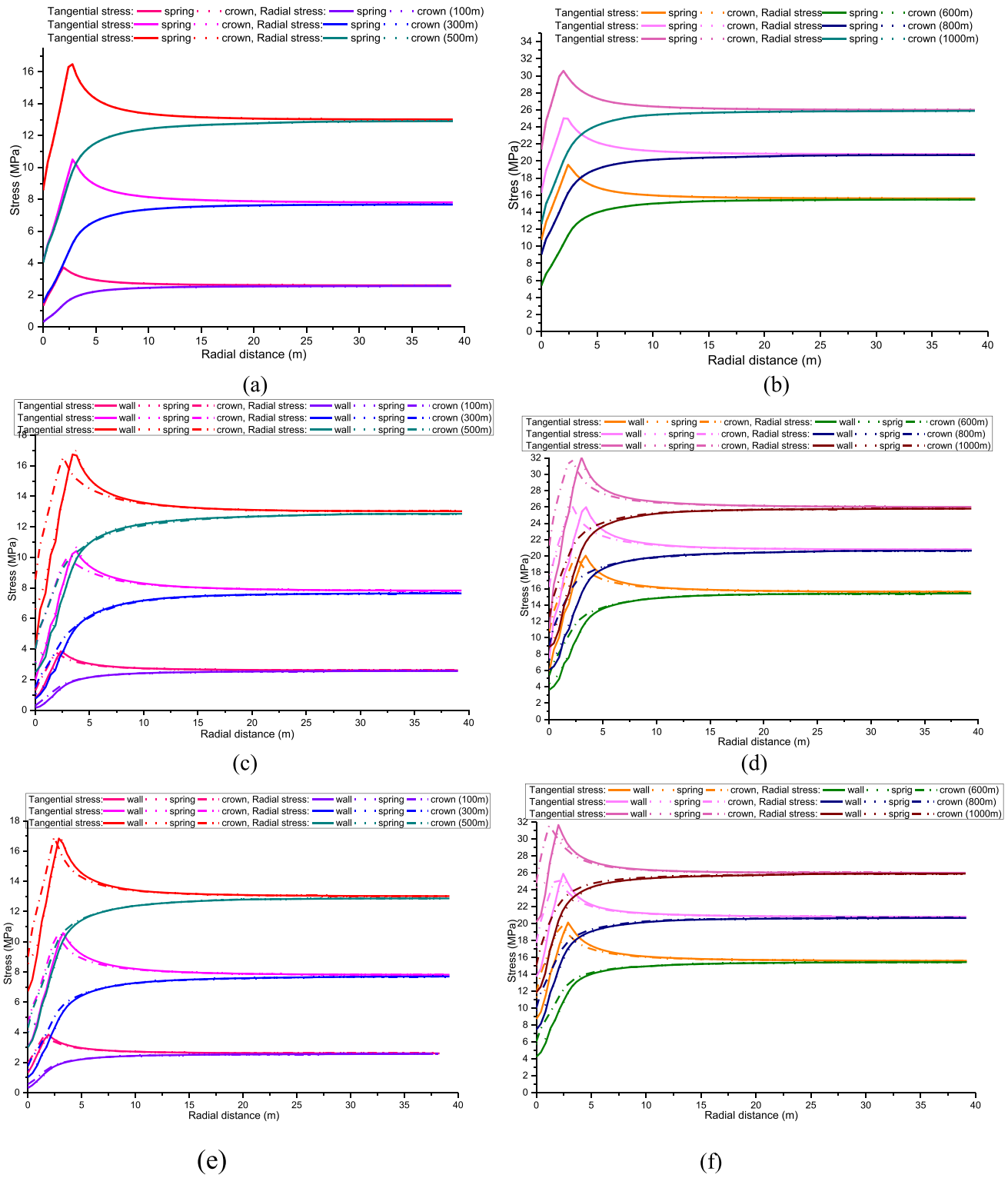

Fig. 14 Tangential and radial stress along the radial distance from tunnel boundary at GSI 10 for **a**, **b** Circular tunnel; **c**, **d** Inverted-D tunnel; **e**, **f** Horse-shoe tunnel

Radial Displacement

Displacements along the radial length for all three tunnel shapes for GSI 10 are shown in Fig. 15. For circular tunnel, displacements are obtained at spring and crown, whereas for inverted-D and horse-shoe tunnel, displacements are

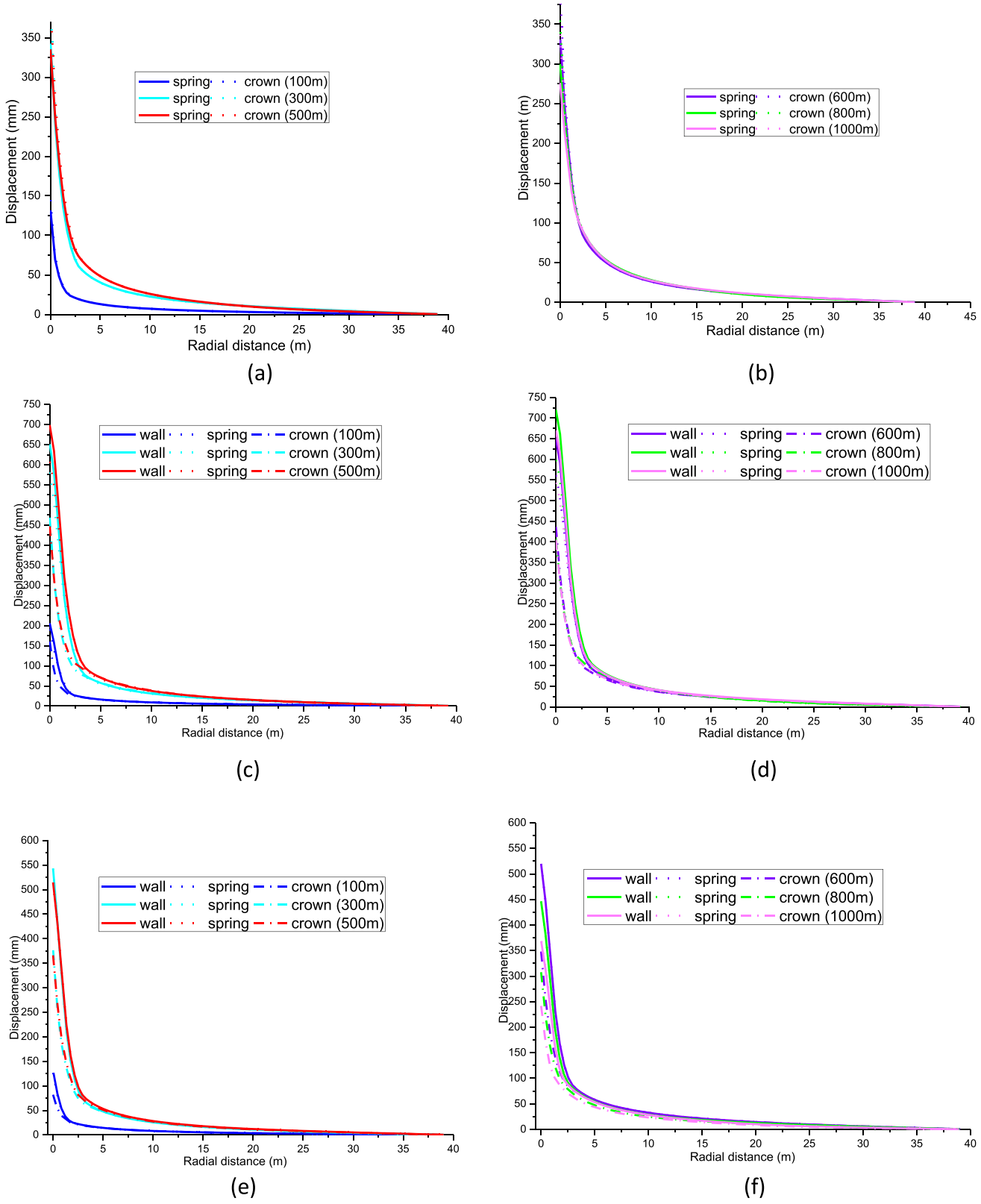

Fig. 15 Displacement along with the radial distance from tunnel boundary at GSI 10 for, **a**, **b** Circular tunnel, **c**, **d** Inverted-D tunnel, **e**, **f** Horse-shoe tunnel

obtained at wall, spring and crown. Observations indicate that the displacement for the circular tunnel at an overburden depth of 100 m is very less, whereas displacements increase for higher overburden depths. Reduction in displacements is observed as GSI of rock mass is increased. Displacement for the circular tunnel at overburden depth of 800 m is 360 m for GSI 10 at tunnel boundary and the displacements are reduced which influences up to ten times the tunnel radius along with radial distance (Fig. 15b), whereas displacement is reduced to 340 m for GSI 30 where its influence in the radial distance of surrounding rock is also reduced to eight times the tunnel radius and further it reduced to 230 m for GSI 40 with the radial distance of four times the tunnel radius. Similar behaviour is observed for inverted-D tunnel and horse-shoe tunnel. For all three tunnel shapes, the influence range of displacement in the surrounding rock is decreasing for higher GSI values. Obtained displacements are higher at the tunnel boundary and further reduced with distance from the tunnel opening.

Conclusions

Numerical analyses are performed by considering a hypothetical model with few assumptions to observe the tunnel behaviour under the influence of material strength, overburden depth and tunnel shapes. Tunnel closure, the radius of the plastic zone and stress distribution in the surrounding rock have been analysed for three tunnel cross sections, namely circular, inverted-D and horse-shoe shape tunnel under isotropic stress conditions for different overburden depths and GSI values. From the obtained results, it was observed that the tunnel shapes influence the tunnel closure. GSI values in another representation of the rock mass structure also exhibit their influence on tunnel behaviour; lesser GSI values exhibit more tunnel closure, whereas higher GSI values show relatively less tunnel closure. The radius of the plastic zone around the tunnel opening indicates the extent of the plastic zone in the surrounding rock mass which results in displacement and stress concentration. The stress distribution in the surrounding rock tunnel and the size of the plastic zone is very important in designing adequate support for the tunnel in squeezing the rock. The shape of the plastic zone for the circular tunnel is different from the inverted-D tunnel and horse-shoe tunnel. A circular shape plastic zone is observed for the circular tunnel, whereas a mushroom shape plastic zone is observed for inverted-D and horse-shoe shape tunnel. It is concluded that the tunnel strain for the circular tunnel is lesser than the horse-shoe shape and inverted-D tunnel, and the radius of the plastic zone is less for circular and horse-shoe shape tunnel when compared to inverted-D tunnel shape. As the stress concentration is higher at sharp edges where the radius of curvature is higher, the inverted-D tunnel and horse-shoe tunnel exhibit higher strain, especially at the invert compared to the circular tunnel. Also, adding to this, the stresses will be uniformly distributed along a circular surface than that of the straight surface (wall and invert in inverted-D and horse-shoe shape tunnel).

When analysing tangential and radial stresses for all the three tunnel shapes, it is observed that the radial stress decreases at the tunnel boundary and approaches to in situ stress value at a certain radial distance away from the tunnel opening. Tangential stresses decrease at the tunnel opening, and within a short distance, it increases above the in situ stress value and then gradually decreases to in situ stress range. This stress redistribution which is also called secondary stresses that occur after tunnel excavation is observed in the zone of plasticity, whereas these stresses reach the primary stress state at the elastic zone in the surrounding rock tunnel. The influence of stress and displacement range along radial distance from tunnel boundary is higher for lesser GSI, whereas its influence in the radial distance reduces as GSI increases. Displacement, the radius of the plastic zone and tangential stress increases as overburden depth increases and reduces as GSI increases. Hence, it is concluded that GSI, overburden depth and tunnel shapes play a major role in the overall behaviour of tunnels in squeezing rock mass. A circular and horse-shoe shape tunnel is suggested in squeezing rock mass to avoid failure.

Further research is required to explore the behaviour of the rock mass up on excavation in squeezing rock subjected to anisotropic stresses including the crucial parameters such as rock mass characteristic, overburden and tunnel shapes.

Funding Authors have not received any funding for the work presented in this research paper.

Declarations

Conflict of interest The authors declare that they have no conflict of interest.

References

1. Barla G (1995) Squeezing rock in tunnels. Int Soc Rock Mech News J 2:44–49
2. Dube AK, Singh B (1986) Study of squeezing pressure phenomenon. Tunn Undergr Space Technol 1:35–39
3. Goel RK, Jethwa JL, Paithankar AG (1995) Tunneling through the young Himalayas—a case history of the Maneri-Uttarkashi power tunnel. Eng Geol 39:31–44
4. Jethwa JL, Dube AK, Singh B Mithal RS (1982) Evaluation of classification system for tunnels in non-squeezing ground

condition. In: Proceeding on rock mechanics, ISRM: caverns and pressure shafts, Rotterdam, pp 607–612
5. Muirwood AM (1972) Ground behavior and support for mining and tunneling. In: Jones MJ (ed) Fourteenth Sir Julius Werner memorial lecture. The Institution of Mining and Metallurgy, London, pp 11–22
6. Wang Y (1996) Ground response of circular tunnel in poorly consolidated rock. ASCE J Geotech Eng 122:703–708
7. Hoek E, Marinos PG (2009) Tunneling in overstressed rock. In: Proceeding on international conference Eurock, ISRM, pp 49–60
8. Lee CF, Sijing W, Zhifu Y (1996) Geotechnical aspect of rock tunneling in China. Tunnel Undergr Space Technol 11:445–454
9. Corkum B, Curran J (1993) Examine3D—stiffness and energy utilities, report to the Mining Research Directorate, Canadian Rockburst Research Program, Department of Civil Engineering, University of Toronto, Publication no. RG-93-09-30, pp 20–27
10. Gioda G, Cividini A (1996) Numerical methods for the analysis of tunnel performance in squeezing rocks. Rock Mech Rock Eng 29:171–193
11. Curran J, Grabinsky M, Corkum B (1994) Numerical analysis of the AECL Mine-by experiment (post construction phase) part 2a—triaxial strain cell results for a circular excavation. Department of Civil Engineering, University of Toronto, Toronto, vol 27,pp 94–102
12. Carranza-Torres C, Fairhurst C (2000) Application of the convergence-confinement method of tunnel design to rock masses that satisfy the Hoek–Brown failure criterion. Tunnel Undergr Space Technol 15:187–213
13. Alejano LR, Alonso E, Rodriguez-Dono A, Fernandez-Manin G (2010) Application of the convergence-confinement method to tunnels in rock masses exhibiting Hoek–Brown strain-softening behavior. Int J Rock Mech Min Sci 47:150–160
14. Brown ET, Bray JW, Ladanyi B, Hoek E (1983) Ground response curves for rock tunnels. J Geotech Eng 109:15–39
15. Chern JC, Yu CW, Shiao FY (1998) Tunnelling in squeezing ground and support estimation. In: Proceeding regional symposium on sedimentary rock engineering, Taipei, pp 192–202
16. Saari K (1982) Analysis of plastic deformation (squeezing) of layers intersecting tunnels and shafts in rock. Dissertation, University of California, Berkeley
17. Singh B, Jethwa JL, Dube AK, Singh B (1992) Correlation between observed support pressure and rock mas quality. Tunnel Undergr Space Technol 7:59–74
18. Singh M, Singh B, Choudhari J (2007) Critical strain and squeezing of rock mass in tunnels. Tunnel Undergr Space Technol 22:343–350
19. Aghda SM, Esmaeil GK, M, (2016) Comparison of squeezibg prediction methods: A case study on Nowsoud tunnel. Geotech Geol Eng Int J 34:1487–1512
20. Itasca Consulting Group, Inc (2011) User manual for FLAC, version 7.0, 5th edn. Itasca Consulting Group, Inc., Minneapolis
21. Hoek E, Carranza-Torres CT, Corkum B (2002) Hoek–Brown failure criterion. In: Proceeding North American rock mechanics society meeting, Toronto
22. Meguid M, Rowe RK (2006) Stability of D-shaped tunnels in Mohr-Coulomb material under anisotropic stress condition. Can Geotech J 43:273–281
23. Lo KY, Lukajic B (1984) Predicted and measured stresses and displacements around the Darlington intake tunnel. Can Geotech J 21:147–165
24. Barla G, Borgna S (2000) Numerical modeling of squeezing behavior in tunnels, Rivista Italiana Di Geotechnical, Department of Structural and Geotechnical Engineering—Politecnico di Torino
25. Barla G (2001) Tunneling under squeezing rock conditions. In: Kolymbas (ed) Proceedings Tunneling mechanics, Eurosummer-School in Tunnel Mechanics, Logos Verlag, Berlin, pp 169–268
26. Dwivedi RD (2013) Prediction of tunnel deformation in squeezing grounds. Eng Geol 161:55–64
27. Panthi KK, Nilsen B (2007) Uncertainty analysis of tunnel squeezing for two tunnel cases from Nepal Himalaya. Int J Rock Mech Min Sci 44:67–76
28. Shrestha GL (2005) Stress-induced problems in Himalayan tunnels with special reference to squeezing. Dissertation, Norwegian university of science and technology, Trondheim
29. Aydan O, Akagi T, Kawamoto T (1993) The squeezing potential of rocks around tunnels: theory and prediction. Rock Mech Rock Eng 26:137–163